OPEN

A novel MRI analysis for assessment of microvascular vasomodulation in low-perfusion skeletal muscle

Eric Zakher[1,2], Tameshwar Ganesh[2] & Hai-Ling Margaret Cheng [1,2,3,4,5]*

Compromised microvascular reactivity underlies many conditions and injuries, but its assessment remains difficult, particularly in low perfusion tissues. In this paper, we develop a new mathematical model for the assessment of vasomodulation in low perfusion settings. A first-order model was developed to approximate changes in T_1 relaxation times as a result of vasomodulation. Healthy adult rats ($N = 6$) were imaged on a 3-Tesla clinical MRI scanner, and vasoactive response was probed on gadofosveset using hypercapnic gases at 20% and 5% CO_2 to induce vasoconstriction and vasodilation, respectively. MRI included dynamic 3D T_1 mapping and T_1-weighted images during gas challenge; heart rate was continuously monitored. Laser Doppler perfusion measurements were performed to corroborate MRI findings. The model was able to identify hypercapnia-mediated vasoconstriction and vasodilation through the partial derivative $\frac{\partial T_1}{\partial t}$. MRI on animals revealed gradual vasoconstriction in the skeletal muscle bed in response to 20% CO_2 followed by gradual vasodilation on transitioning to 5% CO_2. These trends were confirmed on laser Doppler perfusion measurements. Our new mathematical model has the potential for detecting microvascular dysfunction that manifests in the early stages across multiple metabolic and ischemic pathologies.

The microvasculature is a roadway connecting the cells in our body and is the only site where nutrient and waste exchange occurs. It also plays a critical role in maintaining blood pressure and altering local blood supply in response to changing metabolic demands. When the microvasculature becomes dysfunctional, as seen in diabetes and hypertension, this ability to adjust blood supply is compromised. In fact, ample evidence points to microvascular dysfunction as one of the earliest yet undetectable symptoms across a spectrum of conditions, including diabetes, hypertension, obesity, dementia, and coronary artery disease[1-3] – undetectable because a diagnostic technique does not exist for this purpose. Because the vasculature is a connected entity, microvascular pathology is usually not confined to one anatomical location but extends to other tissue beds. Skeletal muscle is one tissue where microvessels are affected across numerous conditions, such as metabolic syndromes (e.g. diabetes, obesity) and neuropathy[4], to name a few. In diabetic patients, for example, exercise intolerance stems from inadequate blood supply to the leg muscle[5]. Identifying skeletal muscle microvascular pathology is, therefore, a potential target for early disease detection.

Imaging muscle microvascular function, however, is challenging. The skeletal muscle bed has a much lower signal compared to other soft tissues when an imaging contrast agent is injected intravenously to fill blood vessels. The lower signal stems from the relatively low perfusion of skeletal muscle, which, at 0.43% of the total cardiac output relative to organ weight, is the lowest of all organs[6]. As such, it is very difficult to sensitively detect vasomodulation-induced dynamic changes in microvascular volume. In a recent innovation described by Ganesh et al.[7], a MRI technique was demonstrated for measuring the dynamics of microvessel modulation in deep organs. Their technique is unique compared to existing clinical methods to assess the microvasculature, because it can isolate strictly changes in microvessel volume and can, therefore, truly measure vasomodulation. In contrast, methods such as laser Doppler flowmetry[8], notwithstanding limited depth penetration, do not specifically measure vasomodulation, because its measurement of perfusion also reflects changes in heart rate. Techniques such as flow-mediated dilation[9] are even less comparable, because those methods assess flow in large arteries, typically the

[1]The Edward S. Rogers Sr. Department of Electrical & Computer Engineering, University of Toronto, Toronto, Canada. [2]Ted Rogers Centre for Heart Research, Translational Biology & Engineering Program, Toronto, Canada. [3]Institute of Biomaterials & Biomedical Engineering, University of Toronto, Toronto, Canada. [4]Heart & Stroke/Richard Lewar Centre of Excellence in Cardiovascular Research, Toronto, Canada. [5]Ontario Institute for Regenerative Medicine, Toronto, Canada. *email: hailing.cheng@utoronto.ca

brachial artery, and not in small vessels. However, in its current form, the approach described in ref. [7] is relatively insensitive to vasomodulation in low perfusion tissue such as skeletal muscle; we need to use the approach as a starting point to build the desired capability.

In this paper, we propose a new analytical method that allows the extraction of microvessel vasomodulation in low perfusion tissue. This method is shown to be sensitive to both vasoconstriction and vasodilation in the microvascular bed of skeletal muscle.

Theory

The intravenous administration of a T_1 contrast agent is used to impart higher signal intensity to tissue; this is achieved through the reduction of T_1 relaxation times of water protons in close proximity to the agent and through the use of T_1-weighted sequences. Tissues that are more richly vascularized will undergo relatively greater contrast enhancement. If the contrast agent remains intravascular, essentially only the blood-pool water protons will experience enhanced relaxation effects. In this scenario, any signal changes in a voxel can be assumed to arise primarily from changes in the vascular volume fraction in that voxel, because this is the only space where the contrast agent resides. In other words, if the vascular volume increases through vasodilation or decreases through vasoconstriction, the T_1 relaxation effect will increase or decrease, respectively – the T_1 relaxation time is effectively dominated by the blood volume fraction.

To appreciate how the blood volume fraction in a voxel is related to the overall T_1, let us examine Eq. (1), which states that the longitudinal relaxation rate ($1/T_1$) is proportional to the concentration of contrast agent in a homogeneous system:

$$\frac{1}{T_1} = \frac{1}{T_{10}} + r_1 C \tag{1}$$

where $1/T_{10}$ is the relaxation rate in the absence of contrast, C is the time-dependent concentration of the contrast agent, and r_1 is a constant for a given contrast agent known as the relaxivity. Since the contrast agent is confined to the vascular space, its concentration in an imaging voxel is simply the contrast concentration in blood (C_b) weighted by the fractional blood volume (v_b). We can rewrite Eq. (1) as follows:

$$\frac{1}{T_1} = \frac{1}{T_{10}} + r_1 C_b v_b \tag{2}$$

The evolution of T_1 with time will be influenced by renal excretion of the contrast agent and any vasomodulation (i.e. changes in v_b) that may be present. To understand this temporal evolution, we take the partial derivative of Eq. (2) with respect to time:

$$\frac{\partial}{\partial t}\left(\frac{1}{T_1}\right) = \frac{\partial}{\partial t}\left(\frac{1}{T_{10}} + r_1 C_b v_b\right) \tag{3}$$

We solve Eq. (3) by taking the quotient rule on the left hand side and the product rule on the right hand side. For practical purposes, we can assume T_{10} is constant with time, as the longitudinal relaxation of tissue with undoped blood changes minimally with blood volume fluctuations[10]. Since both C_b and v_b are time-dependent, the result is:

$$\frac{\partial T_1}{\partial t} = r T_1^2\left(-\frac{\partial C_b}{\partial t}v_b - C_b\frac{\partial v_b}{\partial t}\right) \tag{4}$$

Assuming that the renal elimination rate is a positive-valued constant $K = -\frac{\partial C_b}{\partial t}$ in Eq. (4), we arrive at the following final equation to analyze vasomodulation in low perfusion tissue:

$$\frac{\partial T_1}{\partial t} = r T_1^2\left(K v_b - C_b\frac{\partial v_b}{\partial t}\right) \tag{5}$$

Equation (5) enables us to understand what the partial derivative $\frac{\partial T_1}{\partial t}$ signifies physiologically. Table 1 describes the main scenarios that may arise *in vivo*. We consider each scenario in the following.

Scenarios 1 and 2 represent the simplest case where the renal elimination rate constant K is zero. Although this situation never occurs in practice, it represents the extreme situation where the contrast agent does not leave the body and the blood concentration remains constant. Under these ideal circumstances, positive and negative $\frac{\partial T_1}{\partial t}$ values signify vasoconstriction and vasodilation, respectively, and the magnitude of $\frac{\partial T_1}{\partial t}$ describes how fast vasomodulation occurs.

Scenarios 3 to 5 represent the more realistic situation where renal elimination is present. In the absence of vasomodulation (Scenario 3), $\frac{\partial T_1}{\partial t}$ takes on a positive value, and we do not expect this value to vary with time assuming the elimination rate is approximately constant. The partial derivative $\frac{\partial T_1}{\partial t}$ takes on a negative value (Scenario 4) if only if vasodilation occurs so rapidly that the second term in Eq. (5) dominates the first term. More physiologically relevant, however, is gradual vasodilation, since vessel relaxation is not instantaneous. Here, we should observe an overall increase in the value of $\frac{\partial T_1}{\partial t}$. An initial decrease, if present, arises from a positive $\frac{\partial v_b}{\partial t}$ (i.e.

Scenario	Renal Clearance	Vasomodulation	$\frac{\partial T_1}{\partial t}$	
			Sign	Temporal characteristics
$K=0, \frac{\partial v_b}{\partial t}>0$	No	Vasodilation	Negative	N/A
$K=0, \frac{\partial v_b}{\partial t}<0$	No	Vasoconstriction	Positive	N/A
$K=\text{constant}, \frac{\partial v_b}{\partial t}=0$	Yes	None	Positive	N/A
$K=\text{constant}, \frac{\partial v_b}{\partial t}>0$	Yes	Vasodilation	Negative for rapid changes in v_b	Increasing trend
$K=\text{constant}, \frac{\partial v_b}{\partial t}<0$	Yes	Vasoconstriction	Positive	Decreasing trend

Table 1. Characteristics of the partial derivative in relation to physiological status.

active vasodilation) that reduces the effect of the first term in Eq. (5), whereas the subsequent increase in $\frac{\partial T_1}{\partial t}$ arises from a dilated blood volume fraction (i.e. a higher v_b in the first term now dominates, especially as vasodilation slows down or ceases). Scenario 5 describes vasoconstriction. Since $\frac{\partial v_b}{\partial t}$ is negative, the value of $\frac{\partial T_1}{\partial t}$ can only be positive. As the blood volume fraction decreases, the first term in Eq. (5) decreases, in opposition to the increase exerted by a negative $\frac{\partial v_b}{\partial t}$ in the second term. The direction in which $\frac{\partial T_1}{\partial t}$ changes over this interval depends on the magnitude of the two opposing forces. However, once vasoconstriction has set in and blood vessels are fully constricted, the first term with a reduced v_b dominates and there will be net decrease in the value of $\frac{\partial T_1}{\partial t}$ compared to baseline.

Methods

Animals and controlled gas delivery.
This study was approved by the Lab Animal Services animal care committee at the Hospital for Sick Children (protocol #36668). All procedures were conducted in accordance with the Canadian Council on Animal Care. Male adult Sprague Dawley rats ($N=6$) (Charles River Laboratories), 6 weeks old and weighing 250–300 g, were used. Rats were anesthetized on 3% isoflurane (Forene, Abbott Labs, Baar, Switzerland) in room air (2 L/min flow rate) prior to intubation with a 14-gauge angiocatheter.

A controlled gas mixing circuit described previously[7] was used to deliver graded levels of CO_2 and O_2. The gas blender consisted of a computer-controlled GSM-3 mixer (CWE Inc., Ardmore, PA, USA) and blended O_2, CO_2, and N_2 at a constant total flow of 2 L/min. The output gas mixture was fed first into an isoflurane vaporizer at a flow of 2 L/min and then into an MRI compatible ventilator (MRI-1 Ventilator; CWE, Ardmore, PA, USA). Mechanical ventilation was employed to allow a controlled rate and depth of breathing. The endotracheal tube was connected to a flexible tubing from the gas delivery system. Ventilation was maintained at 70 breaths per minute. Vital signs (heart rate, blood oxygen saturation) of the rat were monitored and recorded using a rodent oximeter and physiological monitor (MouseOX Plus; STARR Life Sciences) mounted on the hind paw. These physiological measurements were taken in real-time to ensure we could monitor the animal's vital signs dynamically. A 27 G angiocath was inserted into the lateral tail vein and connected to a 3-way stopcock for contrast injection during imaging.

During MRI, animals were administered normoxia (21% O_2 room air) to establish baseline. They were then subjected to severe hypercapnia (20% CO_2, 21% O_2, N_2-balanced) followed by mild hypercapnia (5% CO_2, 21% O_2, N_2-balanced).

In-vivo MRI.
Imaging was performed on a 3-Tesla clinical scanner (Achieva 3.0 T TX, Philips Medical Systems, best, The Netherlands), with the animal placed prone on a water blanket (HTP-1500, Adroit Medical Systems, Loudon, TN) set at 38 °C to maintain core body temperature. A receive-only 8-channel wrist coil was used for signal detection. Coronal imaging slices were positioned to include the kidneys and the leg skeletal muscle. Imaging began while animals were on a baseline period of normoxia. After 20 minutes, gadofosveset (0.3 mmol/kg) was administered via tail vein injection. A series of three-dimensional T_1-weighted fast field echo sequences were acquired every two minutes, beginning pre-contrast during the baseline period and continuing throughout the entire examination, with the following sequence parameters: repetition time = 6.11 ms, echo time = 3.23 ms, FA = 20°, number of signal averaging = 2, field of view = 120 mm, thirteen 2-mm thick slices, and 0.6 × 0.6 mm in-plane resolution. Ten minutes after gadofosveset injection, normoxic room air was switched to 20% CO_2, followed 16 minutes later by a switch to 5% CO_2. A four-minute T_1-mapping acquisition was performed prior to gadofosveset administration and repeated prior to every gas transition; the method of Cheng and Wright[11] was used with flip angles (FA) of 2°, 10°, 25°, and 35°. Note that for presentation purposes, we show only imaging data after signal had stabilized after gadofosveset administration.

Laser doppler perfusion measurements.
To validate observations on MRI, real-time laser Doppler perfusion measurements were taken using the OxyFlo (Oxford Optronix Ltd, Oxford, UK) fiber-optic system for all animals. Measurements were in blood perfusion units (BPU), which is a relative quantity of volumetric flow rate. Note that as the catchment volume is approximately 2 mm in diameter and exceeds the spatial dimensions of an individual imaging voxel, the BPU measurement provides a perfusion index equivalent to that averaged over several voxels on MRI. A fiber-optic probe was placed in the leg muscle between the medial and lateral heads of
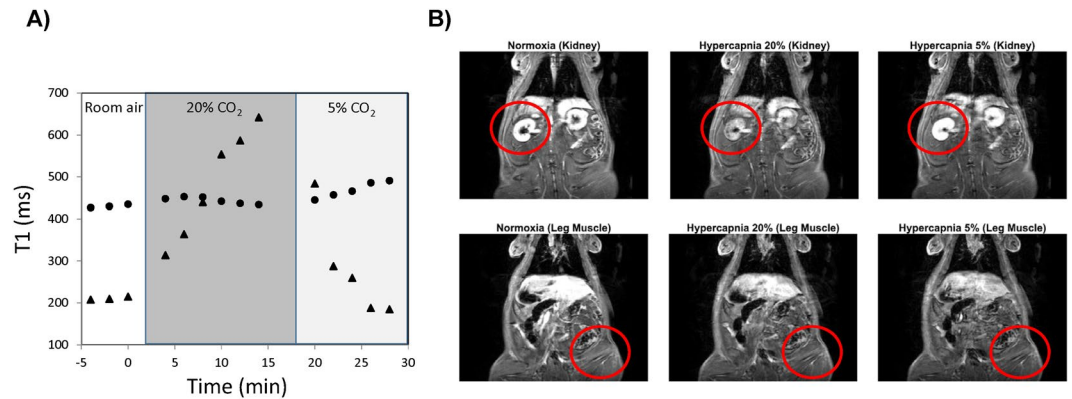
Figure 1. Inadequate sensitivity of T_1 measurements to assess vasomodulation in low perfusion rat skeletal muscle. (**A**) The highly perfused kidney cortex (triangle) exhibits large changes in T_1 in response to hypercapnia, whereas changes in skeletal muscle are very modest (circle). (**B**) Similarly, changes in signal intensity on T_1-weighted images are visible in the kidney but not in the leg skeletal muscle. Red circles are provided to localize the tissues of interest.

the gastrocnemius. Experiments were conducted in the surgical suite of the animal facility instead of the MR suite to ensure sterility. Gas protocols were consistent for MRI and optical measurements.

Data analysis. All data analysis was performed using in-house software developed in Matlab (v.8.3) (Mathworks, Natick, MA). Where T_1-mapping was performed, T_1 relaxation times were calculated at every pixel location across all imaging slices[11]. Regions of interest (ROIs) were outlined on these pixel-wise T_1 maps, in either leg muscle or kidney cortex, to encompass the tissue at multiple contiguous slices. ROIs were tailored to the anatomy of individual animals to ensure that all relevant tissue was included. Care was taken to exclude skin, bone, and major vessels in the ROIs. The ROI-averaged T_1 was then determined. To provide an impression of T_1 variability within these ROIs, in leg muscle the standard deviation was within 10–15% of the mean T_1, while in kidney the standard deviation was within 15–25% of the mean T_1. To calculate T_1-versus-time dynamics over the entire duration of the experiment, signal intensities at remaining time-points were converted to T_1 values via the spoiled gradient echo signal equation, given measured pre-contrast T_1 and post-contrast signal intensity. As before, an ROI-averaged T_1 was calculated for all time-points. The resulting T_1-versus-time curve has a temporal resolution of 2 minutes during individual gas challenge episodes and a four-minute gap where T_1-mapping was acquired. Lastly, the partial derivative of T_1 with respect to time was calculated at all time-points, including the 10-minute normoxic interval before switching to 20% CO_2. A Savitzky-Golay smoothing and differentiation approach was taken to fit the T_1 curve with a second-order polynomial and a 2-point window before computing the derivative. The smoothing helps to reduce the impact of variability in the data points on the computation of derivatives.

Statistics. A one-way ANOVA was used to determine significant changes in $\frac{\partial T_1}{\partial t}$ with respect to time (i.e. twelve time-points) in the leg muscle of all six animals. A Tukey-Kramer test was used for post-hoc analysis. For optical perfusion measurements, the change in perfusion on 20% CO_2 was calculated as the maximum difference in perfusion relative to normoxia and divided by the normoxia perfusion; the change in perfusion on 5% CO_2 was calculated as the maximum difference in perfusion relative to 20% CO_2 and divided by the lowest perfusion during 20% CO_2. A student's t-test was then used to determine significance in perfusion changes. For changes in heart rate, significance was determined using one-way ANOVA, followed by Tukey-Kramer post-hoc analysis, for all gas challenges. Significance is reported at a p-value of 5% for all ANOVA comparisons.

Results

Discerning vasomodulation is difficult in the microvascular bed of tissue with low perfusion, such as skeletal muscle. Whereas the highly perfused kidney exhibits large changes in signal intensity on T_1-weighted images as a result of gas-induced vasomodulation, the magnitude of signal changes in skeletal muscle is much smaller. Quantitative measurement of T_1 relaxation times did not yield a marked improvement in sensitivity to vasomodulation in muscle (Fig. 1).

The proposed analysis of the partial derivative $\frac{\partial T_1}{\partial t}$ dramatically increased sensitivity to vasomodulation in low perfusion tissues. Figure 2 shows the evolution of $\frac{\partial T_1}{\partial t}$ in the absence of gas challenge (i.e. no change in blood volume). A relatively flat profile is clearly evident over the 60-minute observation window, which confirms the assumption of a nearly constant rate of contrast elimination from the body. Figure 3 illustrates the evolution of $\frac{\partial T_1}{\partial t}$ in leg skeletal muscle as its microvasculature responds to gas challenge. Results in the kidney are also shown to provide a reference for interpreting the evolution of muscle $\frac{\partial T_1}{\partial t}$, as renal response to gas challenges is well understood and significant vasoconstriction and vasodilation have been consistently observed in response to 20% CO_2 followed by 5% CO_2[7]. The results in Fig. 2 are presented again in Fig. 3 (shown as dashed lines) to highlight vasomodulation-induced changes against a reference of background contrast elimination. The renal cortical
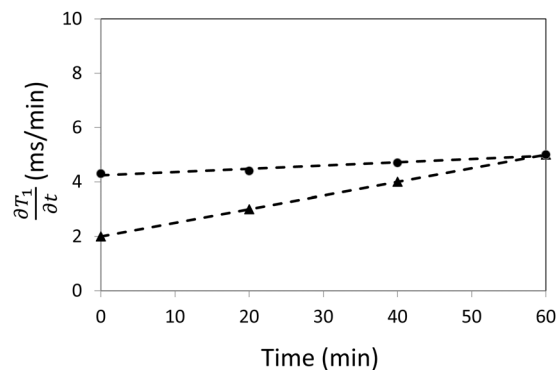
Figure 2. Constant renal elimination rate of contrast agent. Measurements of $\frac{\partial T_1}{\partial t}$ in the absence of gas challenge (i.e. no vasomodulation) in both kidney (triangle) and skeletal muscle (circle) reveal a relatively constant rate of contrast elimination from the body. Note that this protocol is different from the gas challenge protocol used in the remainder of the study. The results shown herein support the validity of the mathematical model proposed for measuring vasomodulation in a low perfusion setting.
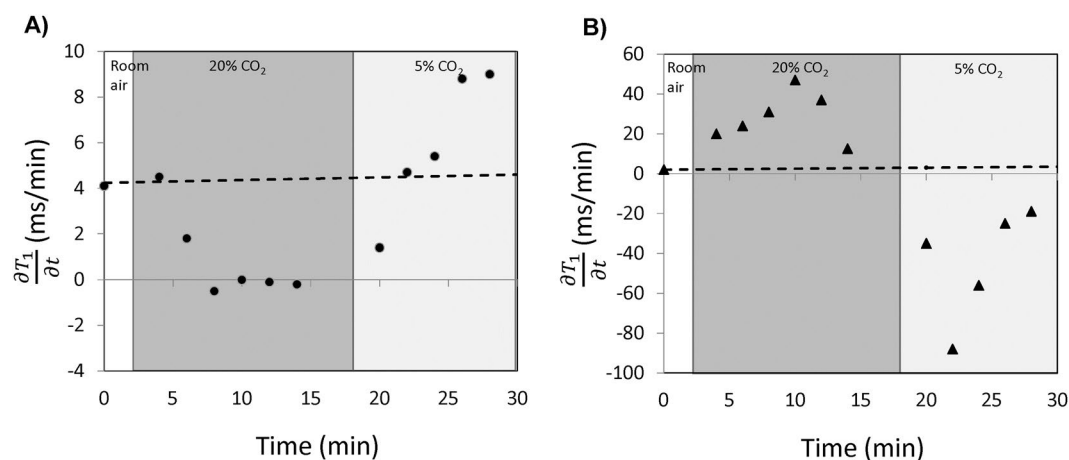
Figure 3. Sensitivity to vasomodulation in low perfusion setting via the parameter $\frac{\partial T_1}{\partial t}$. Data for a representative rat is shown. In leg muscle (**A**), a decreasing $\frac{\partial T_1}{\partial t}$ in response to 20% CO_2 reflects a diminishing blood volume without the rapid vasoconstriction dynamics seen in the kidney cortex (**B**). Upon transitioning to 5% CO_2, an increasing $\frac{\partial T_1}{\partial t}$ reflects an expanding blood volume, again without the rapid vasodilation dynamics of kidney that results in a negative value of $\frac{\partial T_1}{\partial t}$. Dashed lines representing background contrast elimination are also shown for reference.

response is consistent with our mathematical model, where positive values of $\frac{\partial T_1}{\partial t}$ during 20% CO_2 represent vaso-constriction, with the initial increase in $\frac{\partial T_1}{\partial t}$ depicting the effect of active vasoconstriction and the later decrease depicting a slowing down or plateauing of this process. After the switch to 5% CO_2, $\frac{\partial T_1}{\partial t}$ becomes negative as a result of rapid vasodilation. In leg skeletal muscle, the trends observed suggest gradual vasoconstriction ($\frac{\partial T_1}{\partial t}$ remains positive but decreases or stabilizes). In some animals, as seen later in Fig. 4, $\frac{\partial T_1}{\partial t}$ initially spikes above baseline value, indicating immediate vasoconstriction. Upon transition to 5% CO_2, rapid vasodilation is absent (otherwise, $\frac{\partial T_1}{\partial t}$ would become negative as in the kidney), but $\frac{\partial T_1}{\partial t}$ continues to increase, reflecting sustained vaso-dilation on 5% CO_2. Figure 4 summarizes the vasomodulatory responses in the leg muscle of all animals. The overall trend in $\frac{\partial T_1}{\partial t}$ changes was consistent, supporting the robustness of our new method. The decrease in $\frac{\partial T_1}{\partial t}$ in response to 20% CO_2 is significant after 10 minutes on hypercapnia (absolute time is 12 minutes), and the overall increase upon transitioning to 5% CO_2 becomes significant by 4 minutes post-gas transition (absolute time is 22 minutes). Note that in a few animals, $\frac{\partial T_1}{\partial t}$ becomes negative towards the end of 20% CO_2. This reflects an increase in blood volume from perfusion pressure as blood is pushed out of the highly vasoconstricted kidney upstream of the leg muscle.

Figure 5 illustrates a laser Doppler perfusion recording in a representative rat. During the severe hypercapnia interval, perfusion in leg muscle is seen to decrease immediately followed by a gradual increase, which continues upon transition to 5% CO_2. Figure 6 summarizes the perfusion response across all animals, and the trend is in
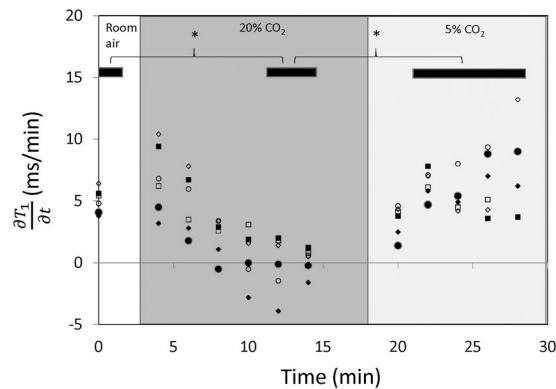
Figure 4. Vasomodulatory response in leg skeletal muscle across all animals. The ability to tease out vasoconstriction and vasodilation in skeletal muscle using the parameter $\frac{\partial T_1}{\partial t}$ is illustrated across all animals. Note the consistency in skeletal muscle vasoreactivity to 20% CO_2 and 5% CO_2. The change in $\frac{\partial T_1}{\partial t}$ is significantly different from baseline normoxia for the last two timepoints on 20% CO_2; $\frac{\partial T_1}{\partial t}$ reverses direction on 5% CO_2, becoming significantly different by 4 minutes after gas transition (*$P < 0.05$). Black bars at the top of the graph indicate the data points where significance was observed.
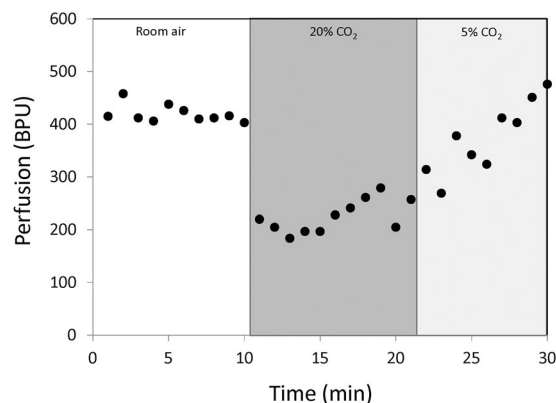

Figure 5. Optical perfusion validation in leg muscle. Laser Doppler perfusion measurements over the course of hypercapnic challenge intervals are shown for a representative rat. Blood perfusion units (BPU) are relative quantities and do not indicate absolute blood flow.
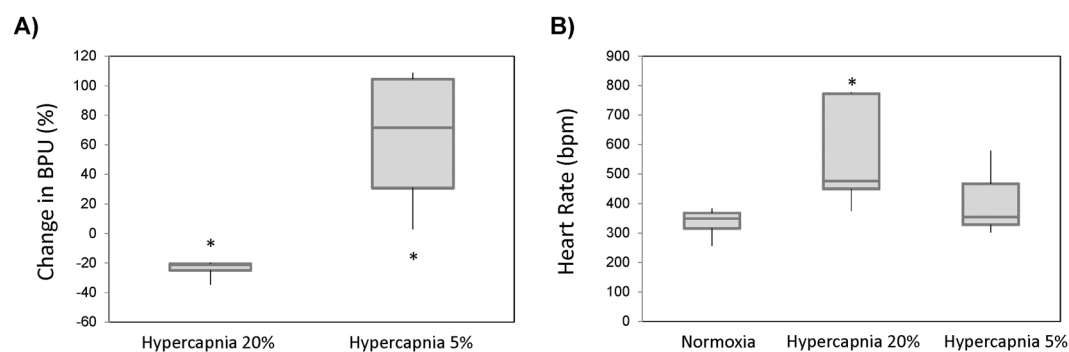

Figure 6. Average changes in perfusion and heart rate in response to severe and mild hypercapnia. (**A**) The maximum perfusion change in leg skeletal muscle induced by 20% CO_2 as measured on laser Doppler and the maximum vasodilation induced by 5% CO_2 are averaged over all animals. (**B**) The average heart rates during normoxia, 20% CO_2, and 5% CO_2 are also shown. Shown are the median, first and third quartile values, and minima and maxima across all animals (*$P < 0.05$).

agreement with MRI: vasoconstriction on 20% CO_2 and vasodilation on 5% CO_2. Note, however, that it is difficult to compare the amplitude of response between optical perfusion measurements and MRI measures of vaso-modulation. This discrepancy arises from the fact that these two metrics are, in fact, different: the MRI metric is

robust against the heart rate variation to which optical perfusion is susceptible. As seen in Fig. 6B, the heart rate increases during 20% CO_2 and decreases during 5% CO_2; these changes counter both the reduction in flow from vasoconstriction during 20% CO_2 and the increase in flow from vasodilation during 5% CO_2. In fact, the observed increased perfusion on optical measurements during the latter phase of 20% CO_2 may be due largely to a much higher heart rate rather than active vasodilation. Therefore, both panels of Fig. 6 must be interpreted together when comparing against MRI measurements.

Discussion

The skeletal muscle microvasculature is involved in numerous pathologies, including ischemia and metabolic syndromes such as diabetes. A technology that opens a window on this system would be invaluable for the early detection of various diseases. Currently, no technology exists to probe the microvasculature non-invasively in deep, low perfused tissue. Specifically, there is no technology to measure vasomodulatory capacity, or vasoreactivity, which is an important index of vascular health and reflects the ability of microvessels to adjust blood flow in response to changing metabolic demands. This paper describes a new analytical method that allows sensitive assessment of microvascular vasomodulation in low perfusion tissue. Compared to assessment of T_1 changes in response to hypercapnia, which have been shown in the literature to be insignificant in skeletal muscle[7], changes in $\frac{\partial T_1}{\partial t}$ are significant. In this study, we showed that the metric $\frac{\partial T_1}{\partial t}$ was sensitive to both vasoconstriction and vasodilation in the leg skeletal muscle, and MRI results were corroborated by invasive Doppler perfusion measurements. Of note is that this new metric works in healthy tissue of normal animals, as demonstrated in this study, and can distinguish unhealthy microvasculature in an injury setting[12].

When interpreting the temporal evolution of the new metric $\frac{\partial T_1}{\partial t}$, one must bear in mind that two discrete influences determine the value of $\frac{\partial T_1}{\partial t}$: the absolute microvascular blood volume at any point in time and the active vasomodulation at that instant in time. MRI results in leg skeletal muscle across all animals revealed a consistent initial decrease in $\frac{\partial T_1}{\partial t}$ immediately after exposure to 20% CO_2 – this decrease is due primarily to an overall reduction in blood volume from vasoconstriction. Halfway through this hypercapnic interval, $\frac{\partial T_1}{\partial t}$ plateaus at a level much lower than normoxic baseline; optical perfusion measurements confirmed a return to increased perfusion at this time. The most likely explanation for this reversal phenomenon is a cessation in the constriction of blood vessels as a result of higher pressure from a greatly elevated heart rate and from blood redistribution arising from renal vasoconstriction. On transition to 5% CO_2, $\frac{\partial T_1}{\partial t}$ continues increasing as blood vessels dilate to accommodate higher perfusion in the presence of a lowered heart rate.

In the kidney, vasoconstriction was also observed during 20% CO_2 followed by vasodilation during 5% CO_2. However, the evolution of $\frac{\partial T_1}{\partial t}$ exhibits a few notable differences. First, upon application of 20% CO_2, several animals demonstrated an initial "hump" in $\frac{\partial T_1}{\partial t}$. This is most likely a result of active vasoconstriction (second term in Eq. (5)) dominating the influence of a lower blood volume (first term in Eq. (5)). Similarly, during the initial interval after the transition to 5% CO_2, the values of $\frac{\partial T_1}{\partial t}$ were negative, which implies active vasodilation to the extent that, again, the second term in Eq. (5) dominates. Another interesting observation is that as renal vasodilation continues during the 5% CO_2 interval, a point is reached where blood is diverted *from* skeletal muscle downstream from the kidney – this is reflected in the plateau/downturn of the $\frac{\partial T_1}{\partial t}$ graph in leg muscle in Fig. 4 and is known as the steal effect.

It is worth noting that a truly equivalent validation method does not exist. In this study, we used optical Doppler perfusion measurements as the best alternative, but like most clinical techniques for assessment of vasomodulation, optical Doppler also evaluates volumetric blood flow and not changes in vessel tone. An increase in perfusion measured on optical Doppler can simply result from a higher heart rate without necessarily changes in vessel diameter. However, when we take in account heart rate variations in our interpretation of Doppler perfusion measurements, we can form a more accurate understanding of vasomodulatory responses. For example, during 20% CO_2, Doppler measurements indicated decreased perfusion at the same time that heart rate was greatly elevated. In the presence of greater perfusion pressure, decreased perfusion can only arise as a result of vasoconstriction.

Our model is a first-order mathematical approximation of the effect of vasomodulation on contrast-induced T_1 effects. It assumes that renal elimination of the contrast agent is constant, but this may be true only over a short time interval and not over the entire duration of the imaging experiment. Future work will model more accurately this elimination profile. The model also is not sensitive to second-order effects that may distinguish more clearly rapid versus slow vasomodulation. In its present form, our model can clearly separate vasodilation from vasoconstriction but cannot ascribe the change to hormonal or neuronal factors[13,14] on the basis of the timing of vasomodulation. Further efforts are required to develop a more complex model that encompasses these elements.

There are several points to consider when implementing the proposed method for assessing microvascular reactivity. First, the measurement duration must be short with respect to the phenomenon of interest. In other words, we must achieve a sufficiently high temporal resolution in our MR acquisition to capture the dynamics of a changing blood volume. Given that vasomodulation occurs on the time scale of minutes, we are well within the required sampling rate. However, while very rapid imaging is unnecessary, it would be beneficial to increase the temporal resolution beyond the 2-minute interval in our current implementation. Doing so would increase the robustness of analyzing the first-order differential of T_1 versus time, as decreased temporal spacing between data-points would improve the accuracy of derivative estimates. It is important to note that the value of $\frac{\partial T_1}{\partial t}$ on either side of a gas transition will have contributions from before or after the transition; this inevitable "artifact" means that the calculated $\frac{\partial T_1}{\partial t}$ values immediately adjacent to a gas transition should be interpreted with caution. With our current temporal sampling every 2 minutes, excluding these transitions points may remove important

information. However, if our data had been acquired at a higher temporal resolution, we could have easily eliminated $\frac{\partial T_1}{\partial t}$ values on either side of a gas transition without sacrificing the time extent over which we characterize $\frac{\partial T_1}{\partial t}$ changes. Another opportunity also arises when the acquisition speed is increased: the proposed analysis approach may be applied on a higher temporal resolution dataset to assess phenomena with rapid dynamics, such as spontaneous vasomotion and pulsatility. The last point to consider is water exchange, which may occur between the intra- and extra-vascular compartments and exert an influence on T_1 measurement. However, water exchange between these compartments has been shown to reside predominantly in the slow regime[15], and the effect on T_1 would be minimal.

A final comment pertains to the study of microvascular dynamics. There is ample literature on the oscillatory nature of microvascular blood flow, with the majority employing optical perfusion methods with a very high temporal sampling rate[16,17]. With such rapid sampling, one can observe a wide frequency range associated with cardiac, respiratory, or myogenic origins. Sophisticated extraction of these distinct frequency components is possible through wavelet analysis and non-linear mode decomposition[17]. These analysis methods may potentially be valuable for analyzing our MRI measurements; to do so, we would need to increase our temporal resolution to exceed at minimum 10 seconds and ideally approach 1 second.

The ultimate utility of the proposed analytical method will rest on its ability to identify diseased or injured microvessels on the basis of their vasomodulatory capacity. There are a number of models to investigate, including ischemic insult, hypertension, and obesity. In ischemic injury where the endothelium is affected, we can expect a reduced capacity to adjust vessel tone compared to healthy microvessels. Future work will focus on a range of microvascular pathologies to validate the general utility of the new method in skeletal muscular disease, cerebrovascular disease, and other pathologies in a low perfusion setting.

There is finally the consideration of eventual translation to humans. The contrast agent employed, gadofosveset, had been FDA and Health Canada approved and was used clinically for several years for MR angiography and cardiac MR exams until it was recently withdrawn due to profitability, not safety, reasons. However, if additional indications that justify the need for blood-pool agents are put forth, the reinstatement of these agents into the clinic is highly probable. Given that all other technical aspects, including the gas challenges, have been shown to be safe in humans, the translational path for the proposed technology is viable.

Conclusions
We have presented a novel analytical method to assess microvascular vasomodulation, or vasoreactivity, in low perfusion tissue. To our best knowledge, this is the only non-invasive, deep-tissue imaging technique of its kind. We have demonstrated the capabilities of this technique in skeletal muscle, which has very low perfusion relative to other organs. The method can be applied to other modestly perfused tissues to investigate pathologies where microvascular dysfunction is an early biomarker of disease or injury.

Data availability
The datasets generated during and/or analysed during the current study are available from the corresponding author on reasonable request.

References
1. Lindner, J. R. Cause or Effect? Microvascular Dysfunction in Insulin-Resistant States. *Circulation Cardiovascular Imaging* **11**, e007725 (2018).
2. Bruno, R. M., Masi, S., Taddei, M., Taddei, S. & Virdis, A. Essential Hypertension and Functional Microvascular Ageing. *High Blood Pressure & Cardiovascular Prevention* **25**, 35–40 (2018).
3. Toth, P., Tarantini, S., Csiszar, A. & Ungvari, Z. Functional vascular contributions to cognitive impairment and dementia: mechanisms and consequences of cerebral autoregulatory dysfunction, endothelial impairment, and neurovascular uncoupling in aging. *Am J Physiol Heart Circ Physiol* **312**, H1–H20 (2017).
4. Barrière, D. A. *et al.* Combination of high-fat/high-fructose diet and low-dose streptozotocin to model long-term type-2 diabetes complications. *Scientific Reports* **8**, 424 (2018).
5. Manrique, C. & Sowers, J. R. Insulin Resistance and Skeletal Muscle Vasculature: Significance, Assessment and Therapeutic Modulators. *CardioRenal Medicine* **4**, 244–256 (2014).
6. Williams, L. R. Reference values for resting blood flow to organs of man. *Clinical Physics and Physiological Measurement* **10**, 187 (1989).
7. Ganesh, T., Estrada, M., Yeger, H., Duffin, J. & Cheng, H. M. A non-invasive magnetic resonance imaging approach for assessment of real-time microcirculation dynamics. *Scientific Reports* **7**, 7468 (2017).
8. Marks, N. J. Quantitative analysis of skin flap blood flow in the rat using laser Doppler velocimetry. *Journal of the Royal Society of Medicine* **78**, 308–314 (1985).
9. Korkmaz, H. & Onalan, O. Evaluation of endothelial dysfunction: flow-mediated dilation. *Endothelium* **15**, 157–163 (2008).
10. Ganesh, T., Estrada, M., Duffin, J. & Cheng, H. L. T2* and T1 assessment of abdominal tissue response to graded hypoxia and hypercapnia using a controlled gas mixing circuit for small animals. *Journal of Magnetic Resonance Imaging* **44**, 305–316 (2016).
11. Cheng, H. L. & Wright, G. A. Rapid high-resolution T(1) mapping by variable flip angles: accurate and precise measurements in the presence of radiofrequency field inhomogeneity. *Magnetic Resonance in Medicine* **55**, 566–574 (2006).
12. Ganesh, T., Zakher, E., Estrada, M. & Cheng, H. M. Assessment of microvascular dysfunction in acute limb ischemia-reperfusion injury. *Journal of Magnetic Resonance Imaging* **49**, 1174–1185 (2019).
13. Elam, M., Yao, T., Thorén, P. & Svensson, T. H. Hypercapnia and hypoxia: chemoreceptor-mediated control of locus coeruleus neurons and splanchnic, sympathetic nerves. *Brain Research* **222**, 373–381 (1981).
14. Sheng, Y. & Zhu, L. The crosstalk between autonomic nervous system and blood vessels. *International Journal of Physiol Pathophysiol Pharmacol* **10**, 17–28 (2018).

15. Carreira, G. C. *et al.* Effects of water exchange on MRI-based determination of relative blood volume using an inversion-prepared gradient echo sequence and a blood pool contrast medium. *Magnetic Resonance Imaging* **27**, 360–369 (2009).
16. Smirni, S., McNeilly, A. D., MacDonald, M. P., McCrimmon, R. J. & Khan, F. *In-vivo* correlations between skin metabolic oscillations and vasomotion in wild-type mice and in a model of oxidative stress. *Scientific Reports* **9**, 186 (2019).
17. Ticcinelli, V. *et al.* Coherence and Coupling Functions Reveal Microvascular Impairment in Treated Hypertension. *Frontiers in Physiology* **8**, 749 (2017).

Acknowledgements

Author contributions

Eric Zakher contributed to (i) conception of the derivative method, (ii) design and execution of *in-vivo* experiments, (iii) analysis of data, (iv) drafting the article, and (v) providing final approval of the version submitted. Tameshwar Ganesh contributed to: (i) design and execution of *in-vivo* experiments, (ii) analysis of data, and (iii) providing final approval of the version submitted. Hai-Ling Cheng contributed to: (i) overall direction, design of experiments, and funding, (ii) derivation of the mathematical model, (iii) design of MR acquisition protocol, (iv) analysis and interpretation of data, (v) drafting and revising the article, and (vi) providing final approval of the version submitted.

Competing interests

The authors declare no competing interests.

Additional information

Correspondence and requests for materials should be addressed to H.-L.M.C.

Reprints and permissions information is available at www.nature.com/reprints.

Publisher's note Springer Nature remains neutral with regard to jurisdictional claims in published maps and institutional affiliations.